nature communications

Article

https://doi.org/10.1038/s41467-025-59057-x

Coarctate reaction for synthesis of fluorescent *N*-heterocycles, late-stage functionalization, and photo-triggered drug delivery

Received: 27 September 2024

Accepted: 10 April 2025

Published online: 22 April 2025

Check for updates

Samrat Sahu[1,2], Zachary E. Paikin[1,2], John M. Talbott[1], Patrick Czabala[1] & Monika Raj[1]

Coarctate reactions, involving the simultaneous formation and cleavage of two bonds at single or multiple atoms, have remained largely unexplored for biomolecular applications. These reactions are characterized by complex helical orbitals in their transition state and produce unique chemical entities unattainable by other methods. This makes coarctate reactions particularly useful for expanding the chemical diversity and properties of biomolecules. In this study, we apply an azo-ene-yne coarctate reaction to synthesize isoindazole-based *N*-heterocycles and explore their biomolecular applications. The azo-ene-yne coarctate method demonstrates high chemoselectivity, thus enabling the synthesis of unnatural amino acids and drug conjugates, and late-stage peptide functionalization. These isoindazole-based *N*-heterocycles exhibit inherent fluorescence, which can be enhanced and red-shifted through electronic tuning. Additionally, we discover a photo-triggered cleavage of the isoindazole moiety from 2-amine-isoindazole, enabling the light-triggered selective delivery of secondary amine and hydroxyl-containing drugs, which represent over 70% of current pharmaceuticals. We also employ a light-triggered method for the selective deprotection of secondary amines and the late-stage functionalization of peptides with isoindazole, enabling access to previously unexplored chemical space.

Linear and cyclic reactions have been extensively used for the modification and late-stage functionalization (LSF) of peptides[1–4], significantly impacting drug discovery by enhancing pharmacological properties like cell permeability, stability, and binding affinity, without the need for laborious de novo synthesis[5–9]. However, while there is a substantial body of literature on modifying biomolecules using linear and cyclic reactions, analogous methods employing the third fundamental reaction topology, coarctate, are notably absent (Fig. 1a). Coarctate reactions offer the potential to generate unique chemical moieties that are unattainable through existing methods, providing access to unprecedented chemical space and properties for biomolecule functionalization[10–16]. Integrating heterocyclic moieties via coarctate reactions could revolutionize modern drug design and discovery, offering avenues for creating advanced therapeutics with enhanced efficacy and specificity[17–20]. A major challenge in pursuing this goal, however, lies in the intricate mechanism of coarctate reactions. This reaction involves the near-concerted breaking and making of two bonds at one atom (or a sequence of atoms) by utilizing helical,

[1]Department of Chemistry, Emory University, Atlanta, GA 30322, USA. [2]These authors contributed equally: Samrat Sahu, Zachary E. Paikin.
e-mail: monika.raj@emory.edu

orthogonal basis orbitals (s and p) in the transition state (Fig. 1a)[13,14,21,22]. Modifying biomolecules in particular presents additional challenges due to their richness in reactive functional groups which must be tolerated during late-stage functionalization.

Here, we have demonstrated that the azo-ene-yne coarctate method—characterized by the reaction of a secondary amine with a 2-alkyne substituted diazonium ion, followed by heterocyclization—produces unique and modifiable 2-amine-isoindazole compounds[10,12] with exceptional chemoselectivity, tolerating all reactive functional groups on peptides. We applied this strategy to synthesize unnatural amino acids and facilitate late-stage peptide functionalization with diverse secondary amines (Fig. 1b). Significantly, we have discovered that the 2-amine-isoindazole heterocycle exhibits inherent fluorescence, which can be further enhanced and red-shifted by tuning the substituents. This feature enables the creation of fluorophores for cellular imaging applications (Fig. 1b). Moreover, we have discovered that the 2-amine-isoindazole heterocycle can be activated by light to selectively release the amine group at specific wavelengths. This led to the development of a precise, photo-triggered approach for selective drug delivery through photolysis of the N-N bond of the 2-amine-isoindazole moiety (Fig. 1b). Given its compatibility with drugs containing secondary amines or hydroxyl groups, this method holds the potential to study over 70% of existing pharmaceuticals and offers advanced therapeutic monitoring. The versatility and innovation of the azo-ene-yne coarctate method highlights its broad utility in investigating a wide array of biological processes within live cells. By offering precise control over the timing and localization of molecule release, this method provides researchers with an unparalleled level of control, facilitating in-depth studies of complex cellular behaviors and molecular interactions[20,23,24].

Results and discussion

Development of a coarctate reaction for biomolecules

At the outset, we selected the azo-ene-yne coarctate approach to modify biomolecules due to the *N*-heterocycle core's prevalence in pharmaceuticals, stemming from its high stability, operational efficiency in the body, and hydrogen bonding capabilities with nucleic acids[17–20,23]. As a first step in pursuing this goal, we optimized the azo-ene-yne coarctate reaction using small molecules. We proceeded with proline methylester-triazene **3a**, synthesized from 2-ethynylaniline **1a** by generating the diazonium ion in situ with $NaNO_2/HBF_4$ and reacting it with *L*-proline methylester **2a** for 1 h (Supplementary Fig. 1). We then optimized the reaction conditions for the azo-ene-yne coarctate reaction on **3a** by varying equiv. of CuCl, solvents, and temperature (Fig. 2a, Supplementary Table 1)[10]. The highest yield (73%) of the 2-amine-isoindazole heterocycle **4a** was achieved with 0.5 equiv. CuCl in 1,2-dichloroethane (DCE) at 50 °C under an oxygen environment (Fig. 2a, entry 5). In contrast, when the reaction was conducted in the presence of air, the yield decreased significantly to 16%, emphasizing the critical role of pure oxygen in achieving optimal results (Fig. 2a, entry 8, Supplementary Table 1). Additionally, the marked reduction in product yield in the presence of water further corroborates that molecular oxygen (O_2), rather than water, is the primary oxidant responsible for aldehyde production (Fig. 2a, entry 7)[21,22].

Substrate scope of coarctate reaction

With optimized conditions in hand for the azo-ene-yne coarctate reaction, we next explored compatibility with varying amines including primary (3-methylbutan-1-amine) and tertiary amines (triethyl amine) (Supplementary Fig. 2). The reaction of the diazonium salt obtained from **1a** demonstrated high selectivity of formation of triazene for secondary amines, as no triazene formation was observed with primary and tertiary amines under the reaction conditions (Supplementary Fig. 2). We next investigated the scope of the triazene formation (Fig. 2b, Supplementary Fig. 3) and coarctate reaction (Fig. 2b, Supplementary Fig. 4) with various secondary amines. The reaction

efficiently proceeded with a range of 5, 6, and 8-membered cyclic amines, yielding compounds **4a**–**4d** in 56–73% yield (Fig. 2b). Spirocyclic and 15-membered crown ethers were also well-tolerated, producing **4e** and **4f** in 70% and 44% yields, respectively. For acyclic amines, both linear and α-branched variants were tested. Branching at the α-center had minimal impact, as compounds **4g**–**4i** formed in 55–60% yields (Fig. 2b). The reaction also successfully accommodated complex acyclic secondary amines with multiple reactive groups, including thienyl, naphthyl, allyl, thiazole, and cyclopropyl functionality (**4j**–**4n**, 34–68% yields, Fig. 2b), highlighting the reaction's robustness and versatility. Attempts to synthesize isoindazole derivatives with ketone handles using internal alkynes from **1b**, via the formation of triazene **3o**, did not yield any product under the optimized reaction conditions. Extended reaction times resulted in the decomposition of the corresponding triazene (Supplementary Fig. 4). The formation of all triazenes (**3a**–**3o**) and 2-amine-isoindazoles (**4a**–**4n**) with various secondary amines was confirmed by ^1H and ^{13}C NMR (Supplementary Figs. 3 and 4). To demonstrate the versatility of the aldehyde handle for various tagging reactions, we successfully employed it to attach alkyne affinity handles to 2-amine-isoindazole **4a** using both oxime and reductive amination chemistries (Supplementary Fig. 4). This strategy enables precise functionalization of the isoindazole scaffold while preserving its structural integrity.

We also evaluated the stability of the 2-amine-isoindazole heterocycle **4a** under various conditions, including acidic conditions (95% trifluoroacetic acid, TFA), basic conditions (90% pyridine, DBU, NaOH), and the two most commonly used bases in solid-phase peptide synthesis (SPPS) (DIPEA and piperidine), as well as under high-temperature conditions (80 °C). Remarkably, **4a** remained stable for over 24 h under all these conditions, highlighting its robustness and suitability for use in harsh and complex environments (Supplementary Fig. 5).

Synthesis of unnatural amino acids using azo-ene-yne coarctate reaction

The broad substrate scope and ability of the azo-ene-yne coarctate reaction to generate stable, unique 2-amine-isoindazole *N*-heterocycles make it well-suited for developing compounds with diverse pharmacological properties. To leverage this, we applied the coarctate reaction to synthesize unnatural Fmoc-amino acids. We started with Fmoc-4-aminophenylalanine, which was esterified and mono-iodinated using *N*-iodosuccinimide (NIS). Following Sonogashira coupling with trimethylsilylacetylene, we performed TBAF-mediated deprotection to obtain compound **5** with a 26% overall yield over 5 steps (Supplementary Fig. 6). Subsequent in-situ diazotization of compound **5** and triazene formation with **2a** yielded Fmoc-triazeneamino acid **6a**. This was then converted into the unnatural Fmoc-2-amine-isoindazole amino acid **7a** using optimized coarctate reaction conditions, achieving a high yield of 76% (Fig. 2c, Supplementary Figs. 7 and 8). We further synthesized a range of unnatural Fmoc-2-amine-isoindazole amino acids (**7b**-**7i**) by varying secondary amines, including cyclic (5 and 8-membered), linear, branched, and functionalized amines with yields ranging from 52 to 82% (Fig. 2c, Supplementary Figs. 7 and 8). To highlight the utility of the unnatural amino acids in peptide synthesis, we used **7b** as a coupling partner for SPPS. The methyl ester group of **7b** was hydrolyzed to generate the Fmoc-amino acid, which was then subjected to the standard Fmoc-SPPS protocol to synthesize the peptide WXHYR (X = isoindazole amino acid) on Rink amide resin. This demonstrates the compatibility of these unnatural amino acids in SPPS and suggests potential applications in genetic code expansion, enabling their incorporation into proteins (Supplementary Fig. 8).

https://doi.org/10.1038/s41467-025-59057-x

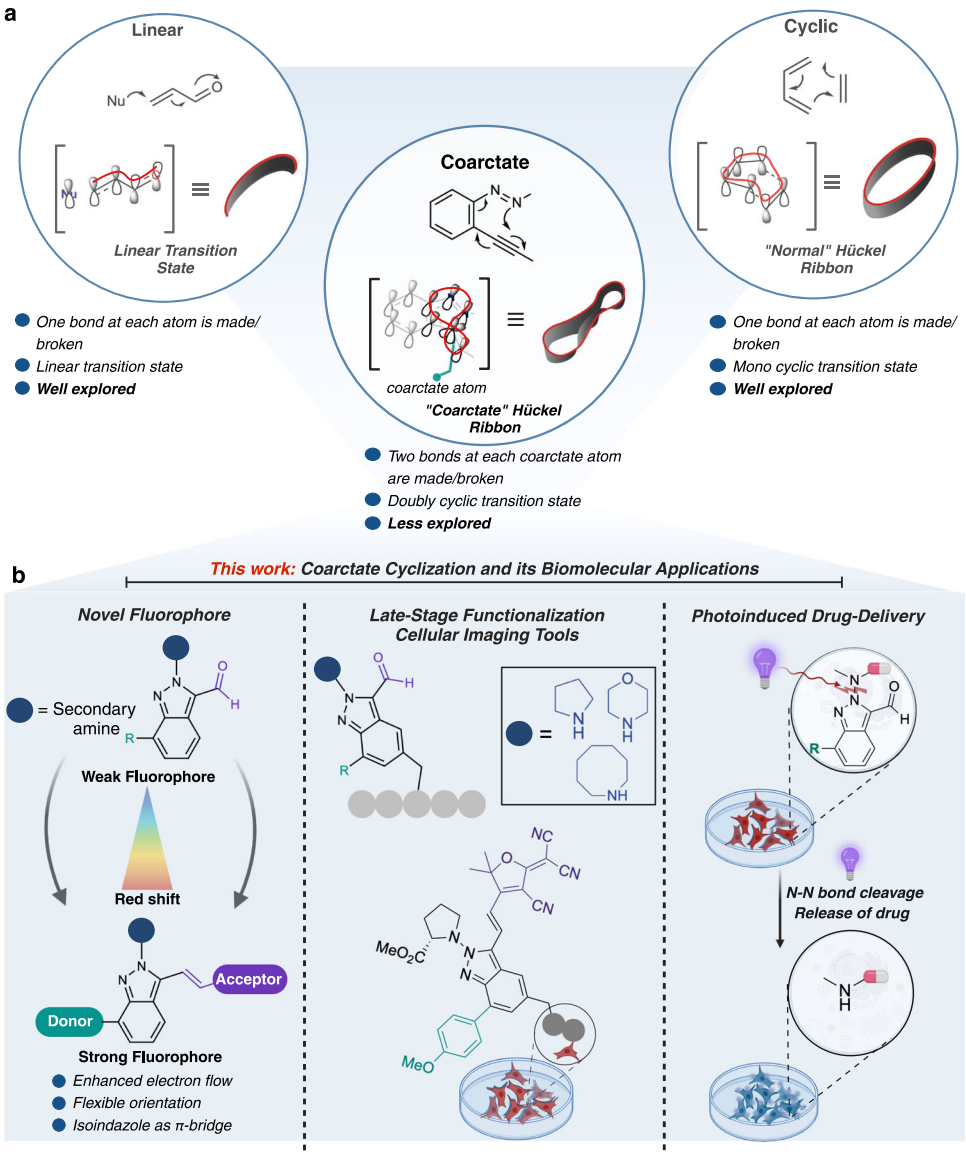

Fig. 1 | Unique transition states and applications of coarctate reaction. **a** Comparison of linear, cyclic, and coarctate reactions. Coarctate reactions feature a unique doubly cyclic transition state that facilitates near-concerted bond formation and cleavage, enabling the generation of chemical moieties with unique properties. **b** Application of the azo-ene-yne coarctate method for developing fluorophores for cellular imaging, synthesizing unnatural amino acids, late-stage peptide functionalization, and photoinduced drug delivery. Created in BioRender. Lab, R. (2025) https://BioRender.com/h97m378.

Tunable fluorescent properties of the 2-amine-isoindazoles

Another notable aspect of the 2-amine-isoindazole core lies in its intriguing photophysical properties. Its rigid planarity and conjugated heterocyclic ring system makes it a promising candidate for fluorescence applications. Additionally, the electronic distribution of the 2-amine-isoindazole offers a versatile platform for tuning its photophysical characteristics. In our pursuit to maximize the potential of the azo-ene-yne strategy, we observed weak fluorescence in compound **4a** (Fig. 3a, λ_{Ab}(**4a**) = 325 nm; λ_{Em}(**4a**) = 401 nm). To enhance fluorescence, we hypothesized that the aldehyde formed during coarctate reaction could be used to extend π-conjugation through olefination, thereby improving fluorescence by modifying the electronic environment of the isoindazole core. We introduced π-conjugated systems such as phenyl (**8**), styryl (**9**), biphenyl (**10**), and 4-nitrophenyl (**11**) at the aldehyde position, which significantly increased fluorescence intensity and redshifted both absorption and emission spectra (λ_{Ab}(**11**) = 404 nm; λ_{Em}(**11**) = 538 nm) (Fig. 3a, Supplementary Fig. 9). However, attempts to shift fluorescence into the near-infrared (NIR) region using stronger electron-withdrawing groups like dicyanomethylene-4H-pyran (DCM, **12**) led to fluorescence quenching. We attribute this quenching to the strong electron-withdrawing nature of DCM, which likely reduced electron density on the isoindazole core, promoting non-radiative decay. Furthermore, moderate electron-withdrawing groups like -CO_2Et (**13**) and -NO_2 (**14**) preserved fluorescence, while the stronger electron-withdrawing dicyano group in **15** caused undesired quenching (Fig. 3a).

To further enhance fluorescence, we focused on modifying specific positions of the isoindazole core that would not interfere with the future incorporation of these fluorophores into peptides. The 7th position was particularly promising due to several factors: (i) it is spatially exposed, unlike the 6th position, which is closer to the peptide backbone; (ii) it allows strategic enhancement of the entire π-conjugated system, improving electron flow across the core; (iii) it offers synthetic accessibility with fewer steps compared to other positions. We explored various electron-donating groups at the 7th position, including 4-*N*,*N*-diphenylaminophenyl (**16**), 4-*N*,*N*-dimethylaminophenyl (**17**), 2-thienyl (**18**), and 4-methoxyphenyl (**19**) (Fig. 3b,

https://doi.org/10.1038/s41467-025-59057-x

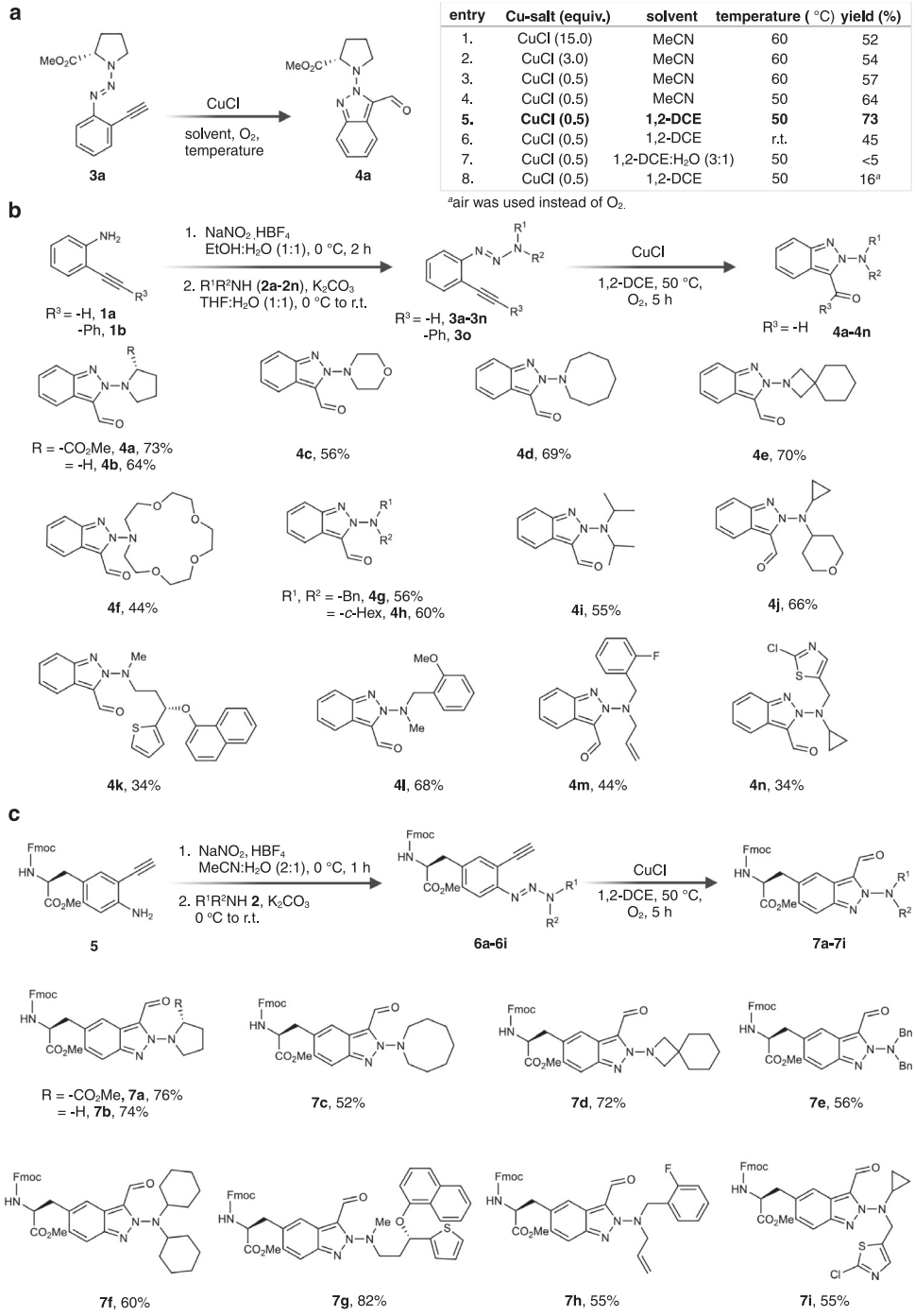

entry	Cu-salt (equiv.)	solvent	temperature (°C)	yield (%)
1.	CuCl (15.0)	MeCN	60	52
2.	CuCl (3.0)	MeCN	60	54
3.	CuCl (0.5)	MeCN	60	57
4.	CuCl (0.5)	MeCN	50	64
5.	**CuCl (0.5)**	**1,2-DCE**	**50**	**73**
6.	CuCl (0.5)	1,2-DCE	r.t.	45
7.	CuCl (0.5)	1,2-DCE:H_2O (3:1)	50	<5
8.	CuCl (0.5)	1,2-DCE	50	16[a]

[a]air was used instead of O_2.

Fig. 2 | Optimization and substrate scope of azo-ene-yne coarctate cyclization for the synthesis of 2-amine-isoindazoles and unnatural amino acids. **a** Optimization of coarctate reaction conditions. Reaction conditions: **3a** (0.2 mmol), and CuCl (equiv. indicated in table) in 1,2-dichloroethane (30 mL) were heated to 50 °C under O_2 atmosphere for the indicated time. Isolated yields are given. **b** Scope of azo-ene-yne coarctate reaction with varying amines, demonstrating robust tolerance for cyclic, acyclic, and complex secondary amines. **c** Generation of unnatural amino acids using coarctate reaction with high yields and broad functional group compatibility. Created in BioRender. Lab, R. (2025) https://BioRender.com/x78n806.

Supplementary Fig. 10). These modifications led to a significant increase in fluorescence compared to the parent compound **4a**, with a slight redshift in absorption (λ_{Ab}(**4a**) = 325 nm to λ_{Ab}(**19**) = 360 nm) and a pronounced Stokes shift (142 nm for **19**). This enhancement is attributed to the extended conjugation of the system. Among the variants, compound **19**, with a 4-methoxyphenyl group attached to the isoindazole ring, emerged as the most promising candidate for further studies due to its higher fluorescence intensity, significant redshift in emission wavelength, and pronounced Stokes shift. To confirm that the observed fluorescence is indeed due to the 2-amine-isoindazole core, we conducted control experiments confirming that analogous diazonium and triazene compounds are non-fluorescent. Only compound **19**, formed exclusively via the coarctate reaction, exhibited good fluorescence (Supplementary Fig. 11). Additionally, we synthesized diazonium and triazene compounds with an aldehyde handle at the ortho position, but did not observe any fluorescence, further emphasizing the crucial role of the isoindazole moiety in providing fluorescence (Supplementary Fig. 11).

https://doi.org/10.1038/s41467-025-59057-x

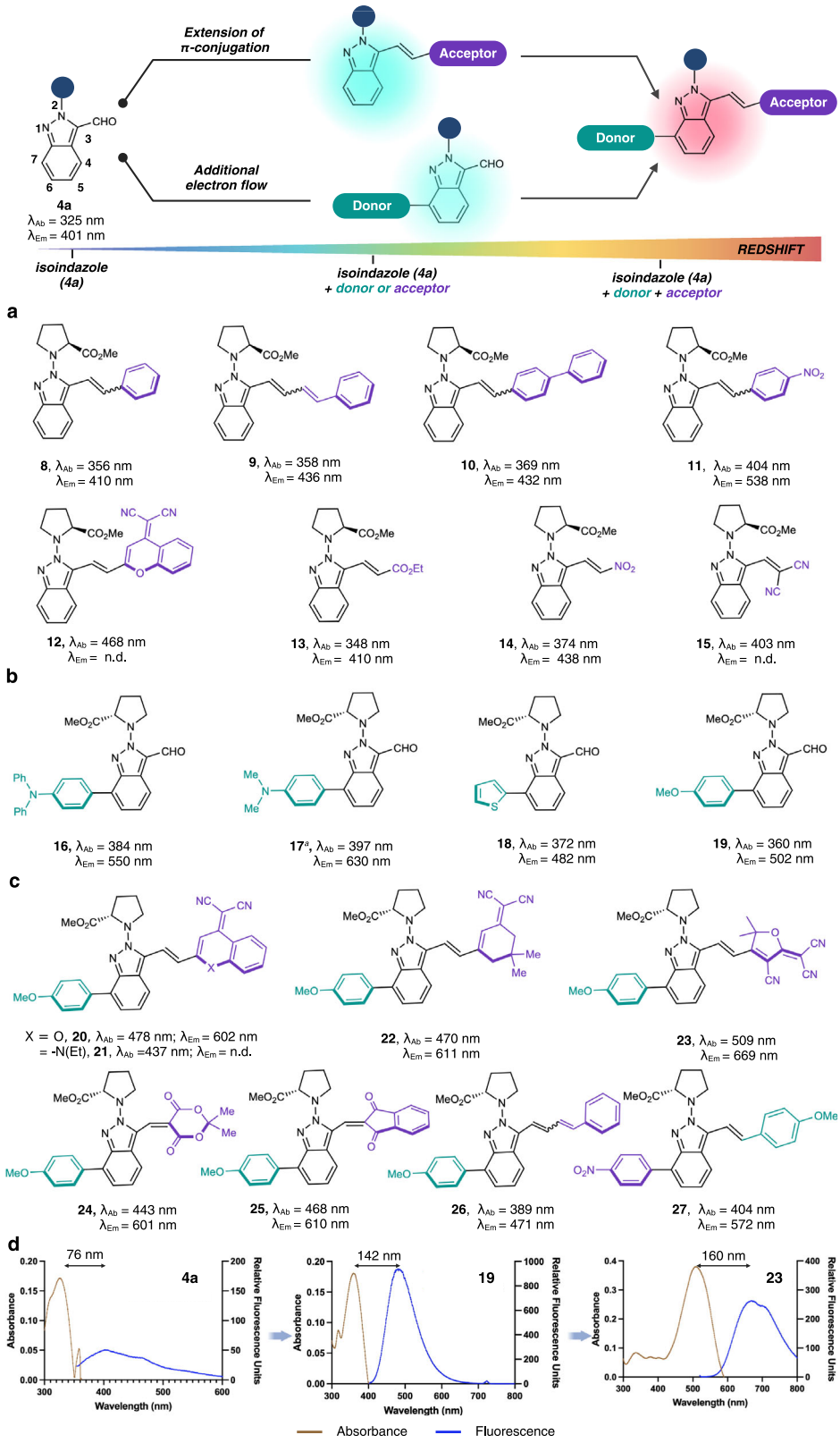

Fig. 3 | Enhanced fluorescent properties of 2-amine-isoindazoles through modification of the electronic environment via conjugating donor-acceptor systems. a Enhanced fluorescence and redshift was achieved through π-conjugation by attaching varying acceptors on 2-amine-isoindazole core. **b** Enhanced fluorescence and redshift was achieved by modifying the 7th position of 2-amine-isoindazole with diverse electron-donating moieties. This also resulted in an improved Stokes shift. **c** Significant changes in fluorescence, Stokes shift, and redshift were achieved by modifying 2-amine-isoindazole with both electron donors at 7th position and electron acceptors at the aldehyde group, with **23** emerging as a standout candidate for NIR fluorescence. **d** Comparison of the excitation and emission spectra for **4a**, **19**, and **23** demonstrating the modular tunability of isoindazole based fluorophores. n.d. not determined. ^{a}Fluorescence recorded in dichloromethane. Source data are provided as a Source Data file. Created in BioRender. Lab, R. (2025) https://BioRender.com/k21m726.

To explore the potential for further redshifting the absorption and emission spectra of our fluorophores, we investigated the intramolecular charge transfer (ICT) mechanism in donor-π-acceptor (D-π-A) systems[25]. The redshift is desirable because it significantly improves imaging by enhancing tissue penetration and reducing phototoxicity and background noise, making it ideal for biological studies[26]. We hypothesized that pairing a donor with an appropriate acceptor at the aldehyde handle could enhance this redshift. We screened various acceptors using 4-methoxyphenyl as the donor, including dicyanomethylene-4H-pyran (DCM, **20**), malononitrile derivatives (**21**–**23**), 1,3-dicarbonyls (**24**–**25**), and styryl groups (**26**) (Fig. 3c, Supplementary Fig. 12). Significant redshifts were observed across all tested acceptors, though some, like **20**, exhibited reduced fluorescence intensity compared to **19**. Notably, **23**, featuring 5,5-dimethylfuran-derived malononitrile, achieved a substantial redshift into the far-red region (λ_{Ab}(**23**) = 509 nm; λ_{Em}(**23**) = 669 nm) while maintaining high fluorescence intensity. Compounds **19** and **23** emerged as the most promising candidates for further use in azo-ene-yne diversified peptides, with **19** and **23** providing desirable fluorescence properties and emission of **23** extending into the NIR region. Quantum yield measurements confirmed their good fluorescent properties (Φ_{19} = 0.06; Φ_{23} = 0.10) (Supplementary Fig. 13), underscoring their potential for applications in peptide modification and cellular imaging. To assess the impact of a secondary amine on the fluorescence profile, we substituted the proline methyl ester in compound **19** with dibenzylamine. While the emission wavelength remained unchanged, a slight reduction in fluorescence intensity was observed with the incorporation of dibenzylamine (Supplementary Fig. 12).

Next, we explored the fluorescence profile of a reversed π-system by attaching 4-methoxyphenyl group (donor) to the aldehyde position via an olefinic linkage and a 4-nitrophenyl group (acceptor) at the C7 position of compound **27**. Our results demonstrate that reversing the donor and acceptor positions preserves the fluorescent properties, with an absorption wavelength (λ_{Ab}) of 404 nm and an emission wavelength (λ_{Em}) of 572 nm (Fig. 3c, Supplementary Fig. 12). Notably, the 2-amine-isoindazole derivatives developed in this study exhibit exceptionally large Stokes shifts: 142 nm for compound **19** and 160 nm for compound **23** (Fig. 3d, Supplementary Fig. 12). These values far exceed those of conventional fluorophores such as Cy2 (~18 nm), BODIPY FL (~9 nm), FITC (~25 nm), and various rhodamine dyes (~25 nm). The large Stokes shifts minimize issues of self-quenching and photobleaching, making these compounds ideal candidates for imaging applications[27–29]. Another key advantage of these isoindazole-based fluorophores is their modular tunability. Both absorption and emission wavelengths can be easily adjusted by swapping substituents on the isoindazole core (Fig. 3d, Supplementary Fig. 12), offering greater flexibility compared to traditional dyes, which have a narrower excitation/emission range and often require more complex synthesis for wavelength tuning. Furthermore, these fluorophores are well-suited for post-synthetic modifications and late-stage diversification, making them more adaptable for a variety of applications.

Peptide diversification by late-stage functionalization using coarctate reaction

Given the potential of the azo-ene-yne coarctate reaction for extensive diversification, we aimed to leverage this method for late-stage functionalization (LSF) of peptides, enabling rapid exploration of structure-activity relationships (SAR) and enhancement of pharmacokinetic and pharmacodynamic properties[1–9]. A critical requirement for LSF of peptides is the compatibility of the method with other reactive amino acids on peptides. To assess the chemoselectivity of the azo-ene-yne coarctate method, we screened decapeptide **28** bearing all reactive functional side chains (Lys, Gln, Tyr, Trp, Cys, Arg, Met, Glu, His, Ser). Diazotization followed by incubation with proline methylester **2a**, as well as exposure to coarctate reaction conditions, resulted in no modifications to peptide **28** (Fig. 4a, Supplementary Fig. 14), demonstrating the high chemoselectivity of the method for secondary amines. Importantly, no oxidation of cysteine (Cys) or methionine (Met) was observed under the reaction conditions. This was further corroborated by performing a similar reaction on another peptide, Ac-RFGKGFC, which also contains Cys (Supplementary Fig. 14). However, it is well-established that more fragile biomolecules, specifically larger proteins, are susceptible to oxidative damage in the presence of Cu/O_2. Oxidation of Cys/Met would pose challenges to applying our chemistry on larger biomolecules, a potential limitation of our method.

We then focused on creating a diverse peptide library through LSF by replacing Tyr in the cytotoxic peptide FIMGPY[30] with *p*-amino-m-alkyne phenylalanine (designated as X) as a Tyr analog. Functionalization of FIMGPX peptide **29** with various cyclic, acyclic, and heterocyclic secondary amines via the azo-ene-yne coarctate reaction yielded a library of 2-amine-isoindazole peptides **31a**–**31d** from corresponding triazenes **30a**–**30d** with high conversions (56–95%) (Fig. 4b, Supplementary Fig. 15). These results underscore the azo-ene-yne coarctate reaction's potential to swiftly diversify peptides by incorporating unique *N*-heterocycles, offering an efficient approach to tune bioactive and cytotoxic sequences for accelerated drug discovery.

Application of coarctate cyclization in developing fluorescent peptides for cellular imaging

We next moved towards integrating fluorogenic 2-amine-isoindazole cores into peptides for cellular imaging. To streamline synthesis, we introduced the *p*-methoxyphenyl donor moiety early, using substituted Fmoc-*p*-amino-*m*-ethynyl phenylalanine (Supplementary Fig. 16). We synthesized triazene from the linear peptide (**32**) and subjected it to the Cu-mediated azo-ene-yne reaction, yielding compound **33** with 70% conversion (Fig. 4c, Supplementary Fig. 17). Next, we functionalized the aldehyde handle of compound **33** with 5,5-dimethylfuran-derived malononitrile to attach the acceptor moiety, aiming to redshift the absorbance and emission. This process furnished compound **34** with 68% conversion. We then evaluated the cellular uptake of peptides **33** (λ_{Ab} = 360 nm; λ_{Em} = 502 nm) and **34** (λ_{Ab} = 510 nm; λ_{Em} = 650 nm) using fluorescent microscopy. Both peptides **33** and **34** showed excellent cellular uptake and fluorescence with minimal background (Fig. 4d, Supplementary Fig. 18). Cellular uptake was further confirmed via flow cytometry (Supplementary Fig. 18). Importantly, neither peptide induced significant cell death in T-47D cells after 2 hours at 100 nM concentration (Supplementary Fig. 18). The fluorescence of peptides **33** and **34** inside cells highlights their stability in biological systems and under fluorescence imaging conditions, demonstrating their potential for effective live-cell imaging without the need for additional fluorophore modifications.

Application of coarctate reaction for the synthesis of drug-isoindazole conjugates for photoinduced drug delivery

Secondary amines and hydroxyl groups are prevalent in various drugs including Ulifloxacin[31], Duloxetine[32], Doxorubicin[33], Endoxifen[33], Norfloxacin[34], and monomethyl auristatin E (MMAE)[35], showcasing diverse biological activities. Given the widespread use of secondary amines in self-immolative (SI) spacers for delivering drugs with hydroxyl groups[36], we explored the azo-ene-yne coarctate method to create drug conjugates for controlled release of both secondary amine and hydroxyl-containing drugs. Our goal was to ensure that therapeutic effects occur only when the drug is efficiently detached from the 2-amine-isoindazole carrier. To ensure the drug conjugate remains stable under physiological conditions and releases the drug only upon activation, we conducted stability tests of compound **4g** at 37 °C in acid, base, PBS buffer (pH 7.4), and serum. No degradation was observed within 24 h, confirming its stability and compatibility for in-vivo applications (Supplementary Fig. 19). For controlled release, we

https://doi.org/10.1038/s41467-025-59057-x

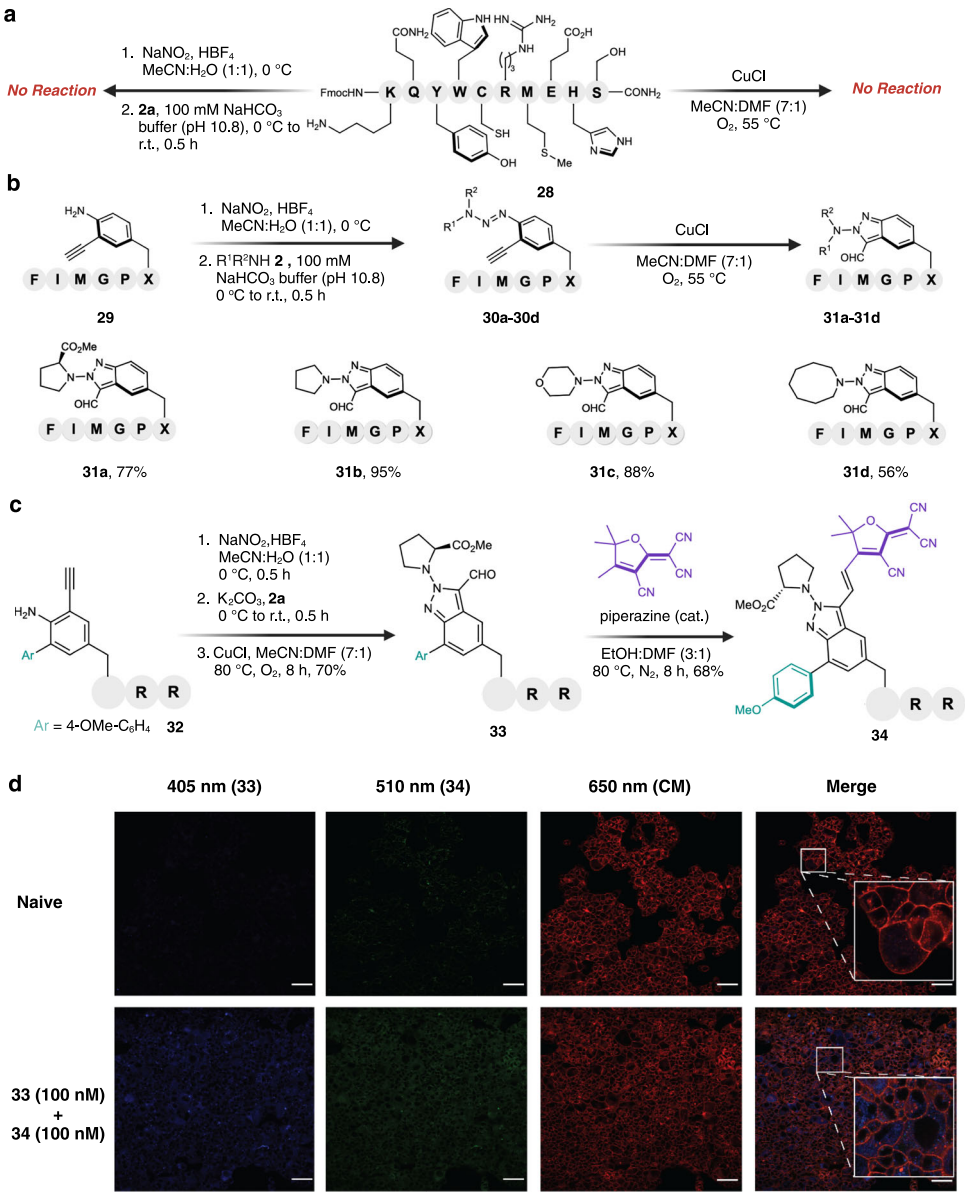

Fig. 4 | Late-stage functionalization and cellular imaging of fluorescent peptides. a Chemoselectivity demonstrated on a model decapeptide **28** with reactive amino acids showing no modification under triazenation and coarctate cyclization conditions, highlighting this method's tolerance of reactive groups. **b** Development of a cytotoxic peptide library through late-stage functionalization, using azo-ene-yne coarctate reaction to incorporate diverse *N*-heterocyclic entities. **c** Cu-mediated azo-ene-yne reaction for the synthesis of 2-amine-isoindazole **33**, followed by the addition of acceptor to aldehyde to yield compound **34** with enhanced and red-shifted fluorescence. **d** Fluorescent microscopy of T-47D cells dosed with 100 nM of peptide fluorophores **33** (λ_{Ab} = 405 nm) and **34** (λ_{Ab} = 510 nm) and stained with deep-red cell mask (CM, λ_{Ab} = 650 nm), demonstrating the potential of azo-ene-yne modified peptides for live-cell imaging. Cells were dosed with **33** and **34** at the same time to demonstrate the red-shifted nature and compatibility of the fluorophores. Naive cells were only stained with cell mask. Scale bar = 20 µm. Repeated on three separate days resulting in consistent imaging results. Source data are provided as a Source Data file. Created in BioRender. Lab, R. (2025) https://BioRender.com/r01k456.

investigated triggers for cleaving the N-N bond of **4g** under biocompatible conditions. Current methods for N-N bond cleavage involve hydrolytically unstable reagents[37], which are not suitable for physiological environments. A promising approach to selectively cleave the N-N bond of 2-amine-isoindazole under biocompatible conditions is by triggering it with biological metabolites already present inside cells, such as reductive or oxidative environments, nitric oxide (NO), or glutathione (GSH). Experiments conducted on model compound **4g**, under various conditions, including treatment with TCEP, H_2O_2, GSH, and NO, did not result in cleavage and degradation of the 2-amine-isoindazole within 24 h, indicating its high stability inside cells (Supplementary Fig. 19). A promising alternative is using light-triggered cleavage (Fig. 5a). Tests conducted with varying wavelengths of light (254–450 nm) on **4g** demonstrated full cleavage of dibenzylamine from 2-amine-isoindazole moiety within 2 h at 302 and 365 nm, while partial release occurred at 450 nm and 254 nm over 5–12 h (Fig. 5a, Supplementary Fig. 20). This N-N bond cleavage not only released dibenzylamine, but also generated NH-free isoindazole **S18** under the photo-triggered conditions, as identified by cleaving **4a** and analyzing isoindazole fragment by NMR (**S18**, Supplementary Fig. 20).

Further investigation into photo-triggered cleavage of substituted **4g** revealed that substituents significantly affect the N-N bond cleavage rate (Supplementary Fig. 21). Converting the aldehyde group of 2-amine-isoindazole to dicyanomethylene-4H-pyran (DCM) or reducing it to an alcohol eliminated cleavage across the 254–450 nm wavelength

https://doi.org/10.1038/s41467-025-59057-x

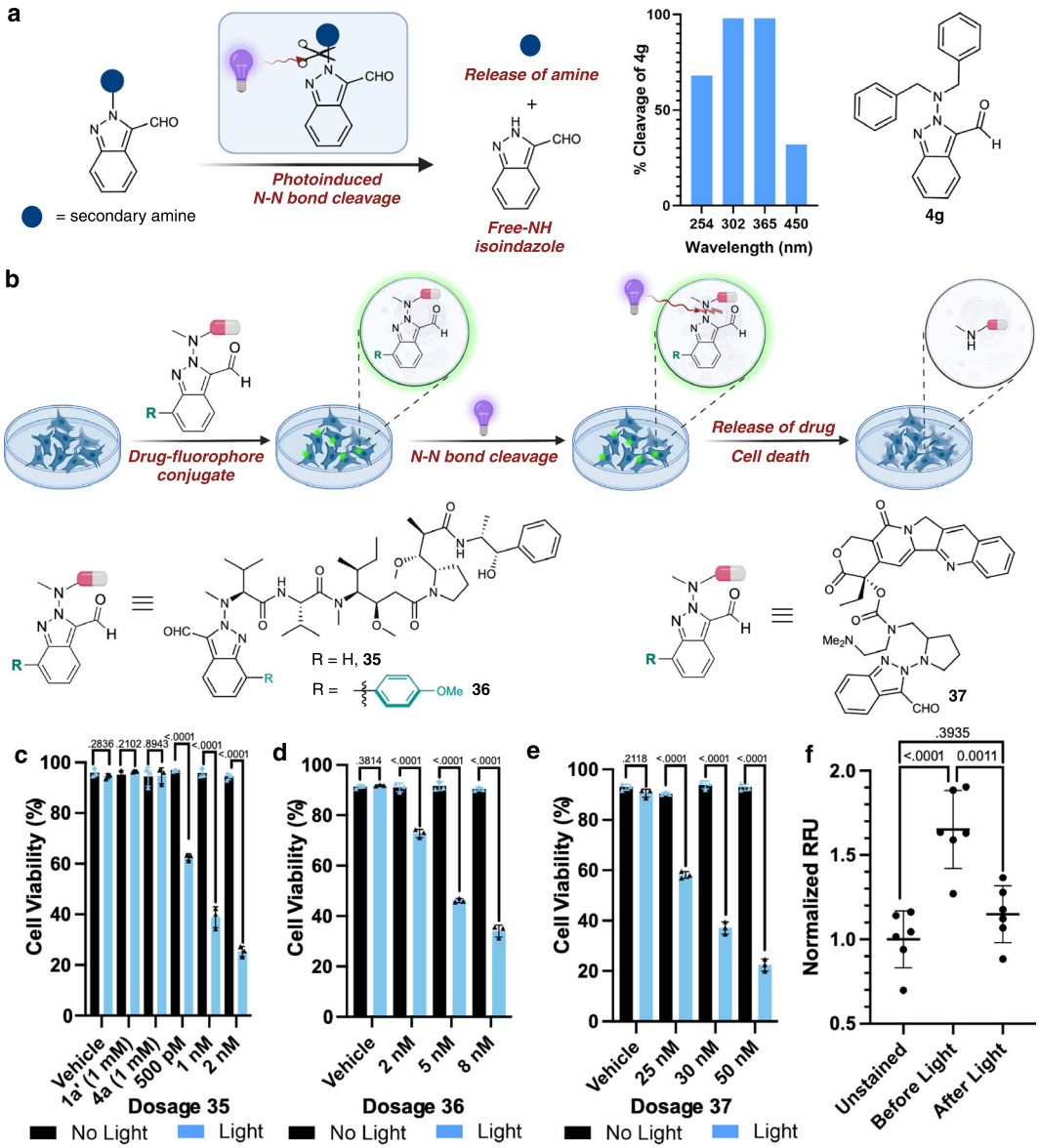

Fig. 5 | Photoinduced controlled release and imaging of drug-isoindazole conjugates. a Photoinduced N-N bond cleavage of fluorogenic 2-amine-isoindazole cores. Screening of various wavelengths for the photoinduced N-N bond cleavage of 2-amine-isoindazole **4g** showed complete release of dibenzylamine within 2 h at 302 and 365 nm. **b** Selective photo-triggered cleavage of 2-amine-isoindazole drug conjugates for drug delivery and structures of drug-isoindazole conjugates **35**–**37**. **c** Cytotoxicity data of **35** at varying concentrations in the presence of 365 nm light in T-47D cells. Significant cell death was observed in the presence of light (blue bars) due to the release of cytotoxic MMAE. No cell death was observed in the absence of light (black bars). Two-sided Student's *t* test was used to determine statistical significance. **d** Cell death of T-47D cells dosed with varying concentrations of **36** in the presence of 370 nm light (blue bars), showcasing the release of cytotoxic MMAE. Two-sided Student's *t* test was used to determine statistical significance. **e** Cell death of HeLa cells dosed with varying concentrations of **37** in the presence of 365 nm light (blue bars), showcasing the release of cytotoxic camptothecin. Two-sided Student's *t* test was used to determine statistical significance. **f** Quantified relative pixel intensity before and after exposure to 370 nm light shows decrease in relative fluorescence of **36** normalized to unstained controls, indicating cleavage of N-N bond of 2-amine-isoindazole core. One-way Anova was used to determine statistical significance. All flow cytometry and imaging experiments were completed in triplicate. All error bars represent mean ± standard deviation. All *P*-values are displayed in each figure. Source data are provided as a Source Data file. Created in BioRender. Lab, R. (2025) https://BioRender.com/f62a768.

range, underscoring the crucial role of the aldehyde group in initiating the cleavage process. We hypothesize that the aldehyde group forms a transient bis-radical species, which plays a key role in driving N-N bond cleavage. To further support the radical mechanism, we incubated **4a** with TEMPO, a radical quencher. No N-N bond cleavage of **4a** was observed in the presence of TEMPO, providing additional evidence that the aldehyde group initiates cleavage through a radical mechanism (Supplementary Fig. 21).

Notably, structurally diverse aldehyde-bearing 2-amine-isoindazoles (e.g., **4a, 16**, and **19**) all undergo N-N bond cleavage at their respective excitation wavelengths for periods greater than 2 h. The substituents on the isoindazole ring, however, influence both the wavelength of light and the time required for N-N bond cleavage. For example, the donor *p*-methoxyphenyl substituted **S25** required longer exposure times and higher wavelengths to achieve full cleavage (5 h and 370 nm, Supplementary Fig. 21). To further validate our proposed mechanism for N-N bond cleavage, we isolated NH-free isoindazoles **S26** and **S27**, obtained from cleaving **16** and **19**, respectively, and characterized the products by NMR (**S26**–**S27**, Supplementary Fig. 22). Interestingly, the strong fluorescence of 2-amine-isoindazoles bearing a *p*-methoxyphenyl group (**19**)

https://doi.org/10.1038/s41467-025-59057-x

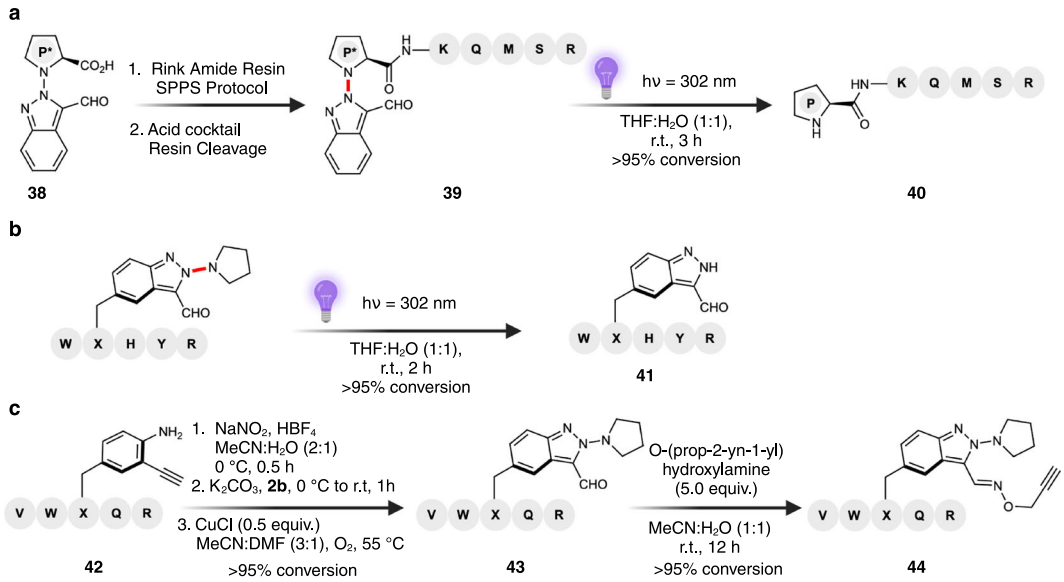

Fig. 6 | Application of coarctate product as photolabile protecting groups, for isoindazole integration, and dual-tagging peptide functionalization. **a** Isoindazole-based photolabile protecting group for secondary amine demonstrating its stability towards acid and selective cleavage by light. **b** Selective photolysis to generate NH-free isoindazole within a peptide, enabling access to indazole amino acids on peptides. **c** Dual-tagging of peptide using azo-ene-yne coarctate cyclization, followed by oxime ligation. Created in BioRender. Lab, R. (2025) https://BioRender.com/q37j452.

diminishes upon N-N bond cleavage following light exposure due to the formation of free isoindazole **S27**. Indeed, isolated NH-free isoindazole **S27** exhibits no fluorescent properties, indicating that cleavage of the N-N bond directly eliminates fluorescence (Supplementary Fig. 22).

To further demonstrate the utility of this N-N bond cleavage, we applied it for the selective release of drugs inside cells. We synthesized three 2-amine-isoindazole drug conjugates using MMAE, a secondary amine-containing cytotoxic drug[35], and camptothecin, a hydroxyl group-containing cytotoxic drug[36]. For camptothecin, we incorporated a proline-containing self-immolative (SI) spacer to add the secondary amine handle (Supplementary Fig. 23)[36,38].

After synthesizing the triazenes, we subjected them to Cu-catalyzed coarctate reaction, yielding 2-amine-isoindazole drug conjugates **35**–**37** with 66–95% conversion (Fig. 5b, Supplementary Fig. 24). With these drug conjugates **35**–**37**, we tested their selective drug delivery efficacy inside T-47D and HeLa cells. We exposed T-47D cells to MMAE-conjugates **35** and **36** at concentrations ranging from 500 pM to 8 nM and HeLa cells to camptothecin-conjugate **36** at concentrations between 25 nM and 50 nM, for 1.5 h (Fig. 5c–e and Supplementary Figs. 25–27). Subsequently, the cells dosed with **35** and **37** were exposed to a 365 nm wavelength of light in a photoreactor for 45 min. Cells dosed with **36** were exposed to two 370 nm Kessil lamps for 1.5 h. A notable increase in cell death was observed over time with increasing concentrations for all compounds. Conversely, in the absence of light, no significant cell death occurred, confirming that the observed cell death was due to the photo-triggered release of the drug. Additionally, we verified that the NH-free isoindazole byproduct **S18**, formed during N-N bond cleavage, is non-toxic to cells; thus, the cell death is due to the impact of drug release (Supplementary Fig. 26).

As anticipated, we observed decreased efficacy for MMAE conjugate **36** compared to analogous MMAE conjugate **35** due to the decreased efficiency of N-N bond cleavage. Additionally, we observed a slower rate of cell death with drug-conjugate **37** (48-h incubation after light treatment) compared to **35** and **36** (24-h incubation after light treatment), attributable to the additional time required for the self-immolative secondary amine spacer to release the hydroxyl drug, camptothecin[36].

Using compound **36**, we visualized MMAE uptake and release in HeLa cells by tracking fluorescence changes upon drug delivery (Supplementary Fig. 28). HeLa cells were incubated with **36** for 1 h at 37 °C, then imaged with confocal microscopy, revealing significant MMAE-conjugate uptake. After exposing the cells to 370 nm light for 1.5 h, confocal microscopy showed a notable reduction in fluorescence, indicating successful drug release (Fig. 5f, Supplementary Fig. 28). It is important to note that the wavelength of light required for fluorescence imaging is the same as that needed for N-N bond cleavage. However, the time required for thorough confocal imaging is less than a few minutes, which is insufficient for N-N bond cleavage to occur, as this process requires a longer exposure time. Given that this method can be applied to drugs containing secondary amines, as well as those with hydroxyl groups, through the formation of secondary amine-containing self-immolative (SI) spacers, it holds the potential to selectively image and study over 70% of drugs currently available on the market under photo-induced biocompatible conditions[23,24]. This approach aligns with other established photo-triggered release systems, such as o-nitrobenzyl and coumarinylmethyl groups, which operate in the UV region and have been widely used for studying biological systems[39].

Isoindazole as selective protecting group for secondary amines

Beyond drug release, we demonstrated the use of photolabile N-N bond cleavage as a selective protecting group for secondary amines (Fig. 6a, Supplementary Fig. 29). We synthesized isoindazole-protected proline **38** and successfully incorporated it into a peptide chain (P*KQMSR-CONH$_2$) containing various acid-labile side-chain protecting groups (Boc, Pbf, Trt, ^{t}Bu) on Rink amide resin, following a standard SPPS protocol. The isoindazole protecting group remained stable during peptide synthesis and during cleavage of peptide from the solid support under acidic conditions. We further subjected the peptide **39** to 302 nm wavelength of light and selectively deprotected the isoindazole group, resulting in >95% conversion to free N-terminal proline-containing peptide **40** (Fig. 6a, Supplementary Fig. 29). This approach offers an alternative to traditional base-sensitive protecting groups (such as Fmoc) in situations where orthogonal deprotection is desired, avoiding the use of harsh reagents. The development of protecting groups that are stable during SPPS and selectively cleaved under mild conditions offers broad potential applications[40]. These include the synthesis of complex peptides and

proteins without damaging sensitive residues, design of prodrugs and controlled drug release systems, and functionalization of surfaces or nanomaterials[41]. They can also be used in the synthesis of natural products and pharmaceuticals, enabling controlled masking and unmasking of functional groups. Additionally, these protecting groups are valuable in creating "smart" materials with stimuli-responsive behaviors in polymer chemistry and diagnostic systems, where they enable the targeted release of agents or signals, improving efficacy and sensitivity[39].

Isoindazole installation in peptides for expanded chemical space

Isoindazole-containing scaffolds are prevalent in numerous marketed drugs and clinical candidates, often imparting enhanced binding affinity, metabolic stability, and desirable pharmacokinetic properties[42]. Despite their widespread occurrence, the direct incorporation of isoindazole moieties into peptides has proven challenging, largely due to the synthetic complexity and lack of mild, chemoselective methods for attaching these heterocycles to a growing peptide chain. To address this, we used WXHYR (X = 2-amine-isoindazole containing amino acid) as a model peptide and applied photolysis to access the free *N*H-free indazole (Fig. 6b, Supplementary Fig. 30). Upon exposure to light (302 nm), the *N*-N bond was selectively cleaved in >95% conversion, liberating the *N*H-free isoindazole **41** (Fig. 6b, Supplementary Fig. 30). This process provides a route to construct isoindazole-containing peptides in a late-stage, high-yield fashion, thereby expanding the chemical space for peptide-based drug discovery. By overcoming the typical synthetic hurdles associated with isoindazole derivatization, our strategy enables controlled insertion of this pharmacologically important motif into peptides or peptidomimetics. This paves the way for next-generation peptide-drug conjugates, where the indazole core can enhance target specificity, and improve metabolic resilience.

To further expand the potential of this azo-ene-yne coarctate cyclization, we performed a dual-tagging of peptides both via secondary amine and the generated aldehyde handle. On a model pentapeptide (VWXQR, **42**, X = *p*-amino-m-alkyne phenylalanine), diazotization, followed by in-situ triazenation with pyrrolidine yielded the corresponding triazene (>95% conversion) (Fig. 6c, Supplementary Fig. 31). Next, treatment of this triazene under Cu-catalyzed coarctate conditions facilitated 2-amine-isoindazole ring formation, delivering **43** with >95% conversion. Finally, we leveraged the aldehyde handle on the newly formed isoindazole moiety to install an alkyne affinity tag via oxime ligation, affording the derivatized peptide **44** with similarly high conversion (>95%) (Fig. 6c, Supplementary Fig. 31). This procedure further confirms that both the secondary amine and aldehyde sites can be used for orthogonal functionalization, opening avenues of our methodology for advanced peptide labeling and dual-tagging applications.

In summary, the azo-ene-yne coarctate method marks a pivotal advancement in the synthesis of unnatural amino acids and late-stage functionalization of peptides. Rather than simply providing a fluorophore-labeling strategy, our work harnesses this underexplored coarctate pathway to establish a versatile platform that enables (i) mild, chemoselective peptide modification, (ii) extensive fluorescence tunability, and (iii) light-driven release of secondary amine- or hydroxyl-based drugs. This innovative approach yields the unique 2-amine-isoindazole heterocycle, a chemical entity not accessible through traditional linear or pericyclic reactions, offering a means to modulate pharmacological properties. The azo-ene-yne coarctate reaction stands out for its exceptional chemoselectivity among reactive functional groups and the intrinsic fluorescence of resulting 2-amine-isoindazole moiety. By fine-tuning the electronic properties of the isoindazole core, we significantly enhanced its fluorescence, achieving emission in the far-red region with minimal toxicity to cells. Of notable importance is the light-activable nature of the 2-amine-isoindazole moiety, which enables (i) selective delivery of secondary amine and hydroxyl group-containing drugs, (ii) the development of selective protecting group for secondary amines, and (iii) the incorporation of free isoindazole into peptides to broaden their therapeutic chemical space. This breakthrough opens avenues for bioimaging and holds substantial promise for accelerating drug discovery, delivery, and development, from cellular diagnostics to therapeutic monitoring.

Methods

General procedure for the synthesis of small molecule 2-amine-isoindazole

Small molecule triazene **3a** (0.2 mmol, 1.0 equiv.) was dissolved in 1,2-DCE or MeCN (30 mL) and CuCl (0.1 mmol, 0.5 equiv.) was added to the reaction mixture. Next, O_2 was bubbled with sonication for 30 min, after which the reaction was left at 50 °C for the indicated time under an O_2 environment. Upon completion by TLC, the reaction mixture was diluted with CH_2Cl_2 (15 mL) and washed with NaCl brine (3 ×50 mL). The organic layer was dried over Na_2SO_4, concentrated, and purified using silica gel column chromatography with an EtOAc:Hexane eluent.

General procedure for the synthesis of unnatural amino acid derivatives

Triazene **6** (0.1 mmol, 1.0 equiv.) was dissolved in 1,2-DCE (10 mL, final concentration 10 mM). The solution was then purged with O_2 for 30 min. CuCl (0.05 mmol, 0.5 equiv) was added to the reaction mixture, which was then heated at 50 °C. Upon complete consumption of the starting material by TLC (4–5 h), the reaction was cooled to room temperature. The crude reaction mixture was purified using silica gel column chromatography with an EtOAc:Hexane eluent to obtain 2-amine-isoindazole **7**.

General procedure for the synthesis of fluorophores 8–11

A 25 mL Schlenk tube was charged with Wittig salt (3.0 mmol, 3.0 equiv.) and backfilled with N_2 thrice. 5 mL of anhydrous toluene was then added under N_2. The resulting mixture was cooled to 0 °C in an ice bath. To this cooled solution, NaH (3.0 mmol, 3.0 equiv., 60% dispersion in mineral oil) was added. The resulting mixture was stirred for 15 min at 0 °C and then brought to room temperature and stirred for an additional 1 h. Aldehyde **4a** (1.0 mmol, 1.0 equiv.) was then added at once and the resulting mixture was heated at 80 °C for 16 h. Upon completion, as indicated by TLC, it was quenched with water and extracted with EtOAc (3 × 5 mL). The combined organic fractions were dried under Na_2SO_4, concentrated and purified using silica gel column chromatography with an EtOAc:Hexane eluent to afford products **8**–**11**.

Synthesis of fluorophore 12

Aldehyde **4a** (27 mg, 0.1 mmol, 1.0 equiv.) and 2-(2-methyl-4H-chromen4-ylidene)malononitrile (27 mg, 0.13 mmol, 1.3 equiv.) were dissolved in anhydrous MeCN (1.0 mL) and 1 drop of piperidine was added. The resulting reaction mixture was heated at reflux. Upon complete consumption of starting material as indicated by TLC, the reaction mixture was cooled down, diluted with EtOAc, and purified using silica gel column chromatography with an EtOAc:Hexane eluent to afford product **12**.

Synthesis of fluorophore 13

A 15 mL Schlenk tube was charged with NaH (24 mg, 0.61 mmol, 2.0 equiv., 60% dispersion in mineral oil) and was backfilled with N_2 thrice. Next, 2 mL of anhydrous THF was added to the tube and it was cooled down to 0 °C using ice bath. Then, triethylphosphonoacetate (136 mg, 0.61 mmol, 2.0 equiv.) was added dropwise to this slurry. After stirring at 0 °C for 15 min, a solution of aldehyde **4a** (83 mg, 0.30 mmol, 1.0 equiv.) in 1 mL anhydrous THF was added dropwise at 0 °C. After 15 min, the reaction was brought to room temperature and stirred for

1 h. The reaction was quenched using water and extracted with EtOAc (3 × 3 mL). The combined organic layers were dried using Na_2SO_4, concentrated, and purified on silica gel column chromatography with an EtOAc:Hexane eluent to afford product **13**.

Synthesis of fluorophore 14
To a solution of aldehyde **4a** (27 mg, 0.1 mmol, 1.0 equiv.) in CH_3NO_2 (1 mL) was added NH_4OAc (15 mg, 0.2 mmol, 2.0 equiv.). The resulting mixture was heated at 90 °C for 1 h. The crude mixture was directly purified on silica gel column chromatography with an EtOAc:Hexane eluent to afford product **14**.

Synthesis of fluorophore 15
A mixture of **4a** (54 mg, 0.2 mmol, 1.0 equiv.) and malononitrile (33 mg, 0.5 mmol, 2.5 equiv.) were dissolved in EtOH (5 mL). 2–3 drops of piperidine were added. The reaction mixture was heated at 90 °C for 1 h. The reaction was quenched, extracted with EtOAc, dried with Na_2SO_4, and purified on silica gel column chromatography with an EtOAc:Hexane eluent to afford product **15**.

General procedure for the synthesis of fluorophores 16–19
A 50 mL Schlenk tube was charged with methyl (7-bromo-3-formyl-2*H*-indazol-2-yl)-*L*-prolinate (700 mg, 2.0 mmol, 1.0 equiv.), arylboronic acid (3.0 mmol, 1.5 equiv.), $Pd(Ph_3P)_2Cl_2$ (140 mg, 0.2 mmol, 10 mol%), and Cs_2CO_3 (10.0 mmol, 5.0 equiv.). Then, 10 mL of degassed 1,4-dioxane:H_2O (9:1) was added. The resulting mixture was heated at 90 °C for 2 h. Upon cooling to room temperature, EtOAc (20 mL) was added. The reaction mixture was washed with H_2O, dried over Na_2SO_4, and purified using silica gel column chromatography with an EtOAc:Hexane eluent to obtain arylated products **16**–**19**.

General procedure for the synthesis of fluorophores 20–25
A 25 mL Schlenk tube was charged with **19** (75 mg, 0.2 mmol, 1.0 equiv.) and acceptor group (0.6 mmol, 3.0 equiv.), dissolved in anhydrous MeCN (2.5 mL). 1–2 drops of piperidine were added, and the resulting reaction mixture was heated at 80 °C. Upon completion, the reaction mixture was cooled down to room temperature and purified using silica gel column chromatography with an EtOAc:Hexane eluent to afford **20**–**25**.

General procedure for late-stage diversification of peptides using coarctate reaction
1 mg (1.0 equiv.) of triazene peptide, FIMGPX, **29** was dissolved in 7:1 MeCN:DMF (7:1, 240 µL). Next, CuCl (0.6 equiv.) was added to the vial from a freshly prepared stock solution (20 µL). O_2 was bubbled for 5 min, after which the mixture was heated to 55 °C and left under an O_2 environment for 5 h. The reaction was analyzed via HPLC (0–80% B over 30 min, solvent B: 0.1% formic acid in MeCN, flow rate: 1 mL/min) and MS to determine the conversion to 2-amine-isoindazole peptides **31**.

Synthesis of 2-amine-isoindazole 33
Triazene (5 mg, 1.0 equiv.) was dissolved in MeCN:DMF (7:1, 2.2 mL, final concentration 3 mM). Next CuCl (3.0 equiv., 400 µL from 50 mM stock solution in MeCN) was added to it and the resulting mixture was heated at 80 °C for 8 h under O_2 atmosphere. The conversion to **33** was determined by HPLC (0–70% B over 30 min, solvent B: 0.1% formic acid in MeCN, flow rate: 1 mL/min) and characterized by MS.

Synthesis of 34 by knoevenagel condensation
33 (1 mg, 1.25 µmol) was dissolved in EtOH:DMF (3:1, 280 µL) and to it was added 1-2 mg of piperazine and 2-(3-cyano-4,5,5-trimethylfuran-2(5H)-ylidene)malononitrile (3.0 equiv., 120 µL from 30 mM stock solution in 3:1 EtOH:DMF). The resulting reaction mixture was heated at 80 °C under N_2 for 8 h. The crude mixture was analyzed by HPLC (0–70% B over 30 min, solvent B: 0.1% formic acid in MeCN, flow rate: 1 mL/min) to determine the conversion to **34** and the product was characterized by MS.

Procedure for live-cell imaging of coarctate fluorescent peptides 33 and 34
Live T-47D cells were plated in an IBIDI 8-well glass bottom chamber at a density of 25,000 cells per well in media and allowed to adhere overnight at 37 °C, 5% CO_2. Cells were treated with 100 nm of **33** and **34** in 200 µL of media and incubated for 1 h before media was removed and cells were washed with 200 µL of PBS for 5 min. PBS was removed and Deep Red Cell Mask (ThermoFischer, C10046) was added according to manufacturer protocol, and cells were incubated for 10 min before being washed with 200 µL of PBS for 5 min (repeated 3 times). 200 µL of fresh media was added and cells were imaged on a Stellaris® 8 Leica DMi8 microscope (20x objective) with fast lifetime contrast (FALCON) module. Samples were excited using a 40 MHz pulsed white light laser tuned to 405, 510, and 650 nm with sequential acquisition. Emitted photons were detected using HyD® S and HyD® X (GaAsP hybrid photocathode). Images were processed and analyzed using ImageJ software.

General procedure for the photo-induced cleavage of N-N bond 2-amine-isoindazole
2-amine-isoindazole **4g** (5 mg, 14.6 µmol) was dissolved in H_2O:THF (1:1, 1 mL) and the reaction was irradiated by a UV lamp at the designated wavelength at room temperature. The reactions were analyzed via HPLC at the specified time to determine conversion to cleaved dibenzylamine (0–80% B over 30 min, solvent B: 0.1% formic acid in MeCN, flow rate: 1 mL/min).

Procedure for the synthesis of MMAE-isoindazole conjugate 35
Triazene MMAE conjugate (5 mg, 5.8 µmol, 1.0 equiv.) was dissolved in 1 mL of anhydrous MeCN and to it CuCl (2.9 mg, 29.0 µmol, 5.0 equiv.) was added. Next, O_2 was bubbled through the reaction mixture for 5 min, after which the vial was heated to 50 °C under an O_2 environment for 4 h. The reaction was analyzed via HPLC (0–80% B over 30 min, solvent B: 0.1% formic acid in MeCN, flow rate: 1 mL/min) to determine the conversion and **35** was characterized by MS.

Synthesis of camptothecin-isoindazole conjugate 37
Triazene Camptothecin conjugate (5 mg, 7.4 µmol, 1.0 equiv.) was dissolved in 1 mL of anhydrous MeCN and to it CuCl (3.7 mg, 37.1 µmol, 5.0 equiv.) was added. Next, O_2 was bubbled through the reaction mixture for 5 min, after which the vial was heated to 50 °C under an O_2 environment for 4 h. The reaction was analyzed via HPLC (0–80% B over 30 min, solvent B: 0.1% formic acid in MeCN, flow rate: 1 mL/min) to determine the conversion and **37** was characterized by MS.

Procedure for the selective delivery of MMAE by photocleavage of MMAE-isoindazole conjugate 35
T-47D cells were dosed with varying concentrations of MMAE-isoindazole **35** for 1.5 h, exposed to 365 nm light for 45 min in the photoreactor, incubated for 24 h, then analyzed by flow cytometry using AV/PI staining (FITC Annexin V purchased from Biolgened, Catalog No. 640945, Lot No. B404229). Vehicle was dosed with concentration of DMSO equivalent to concentration used for largest dosage of **35**. Data is an average of 3 replicates analyzed on separate days using different passage number of cells. Two-sided Student's *t* test was used to determine significance. All error bars represent mean ± standard deviation.

Procedure for the selective delivery of MMAE by photocleavage of MMAE-isoindazole conjugate 36
T-47D cells were dosed with varying concentrations of **36** for 1.5 h in the incubator, exposed to 370 nm Kessel lamps for 1.5 h, incubated

for 48 h, then analyzed by flow cytometry using AV/PI staining (FITC Annexin V purchased from Biolgened, Catalog No. 640945, Lot No. B404229). Vehicle was dosed with concentration of DMSO equivalent to concentration used for largest dosage of **36**. Data is an average of 3 replicates analyzed on separate days using different passage number of cells. Two-sided Student's *t* test was used to determine significance. All error bars represent mean ± standard deviation.

Procedure for the selective delivery of camptothecin by photocleavage of camptothecin-isoindazole conjugate 37

HeLa cells were dosed with varying concentrations of Camptothecin-isoindazole **37** for 1.5 h in the incubator, exposed to 365 nm light for 45 min in the photoreactor, incubated for 48 h, then analyzed by flow cytometry using AV/PI staining (FITC Annexin V purchased from Biolgened, Catalog No. 640945, Lot No. B404229). Vehicle was dosed with concentration of DMSO equivalent to concentration used for largest dosage of **37**. Data is an average of 3 replicates analyzed on separate days using different passage number of cells. Two-sided Student's *t* test was used to determine significance. All error bars represent mean ± standard deviation.

Procedure for the live-cell imaging with MMAE-isoindazole conjugate

Live T-47D cells were plated in an IBIDI 8-well glass bottom chamber at a density of 25,000 cells per well in media and allowed to adhere overnight at 37 °C, 5% CO_2. Cells were treated with 100 nm of MMAE-isoindazole conjugate, **36**, in 200 μL of media and incubated for 1 h before media was removed from half of the wells and washed with 200 μL of PBS for 5 min. PBS was removed and Green Cell Mask (ThermoFischer, C37608) was added, and cells were incubated following manufacturer protocol for 10 min before being washed with 200 μL of PBS for 5 min (repeated 3 times). 200 μL of fresh media was added and cells were imaged on a Stellaris® 8 Leica DMi8 microscope (20x objective) with fast lifetime contrast (FALCON) module. Samples were excited using a 40 MHz pulsed white light laser tuned to 405 nm. Emitted photons were detected using HyD® X (GaAsP hybrid photocathode). Immediately following imaging, the 8-well plate was treated with 370 nm light from two Kessel lamps for 1.5 h. Media was removed from remaining wells (those not stained with cell mask initially) and washed with 200 μL of PBS for 5 min. PBS was removed and Cell Mask was added, and cells were incubated for 10 min before being washed with 200 μL of PBS for 5 min (repeated 3 times) before addition of 200 μL of fresh media and immediate imaging on the Stellaris microscope. Images were processed and analyzed using ImageJ software to determine pixel intensity per cell. Biological replicates were performed on three separate days. Outlier test was performed before data was normalized to unstained wells. One-sided Anova was used to determine statistical significance. All error bars represent mean ± standard deviation.

Reporting summary

Further information on research design is available in the Nature Portfolio Reporting Summary linked to this article.

Data availability

All data supporting the findings of this study are available within the Supplementary Information and from the corresponding author upon request. These include the optimization of the azo-ene-yne coarctate reaction on small molecules and amino acids, peptide diversification, fluorophore synthesis, drug conjugate synthesis, cellular imaging, flow cytometry, and characterization of all synthesized compounds by NMR, HPLC, LCMS, and/or HRMS. Source data are provided with this paper.

References

1. Börgel, J. & Ritter, T. Late-stage functionalization. *Chem* **6**, 1877–1887 (2020).
2. deGruyter, J. N., Malins, L. R. & Baran, P. S. Residue-specific peptide modification: a chemist's guide. *Biochemistry* **56**, 3863–3873 (2017).
3. Lin, S. et al. Redox-based reagents for chemoselective methionine bioconjugation. *Science* **355**, 597–602 (2017).
4. Wang, W., Lorion, M. M., Shah, J., Kapdi, A. R. & Ackermann, L. Late-stage peptide diversification by position-selective C-H activation. *Angew. Chem. Int. Ed.* **57**, 14700–14717 (2018).
5. Henninot, A., Collins, J. C. & Nuss, J. M. The current state of peptide drug discovery: back to the future? *J. Med. Chem.* **61**, 1382–1414 (2018).
6. Cernak, T., Dykstra, K. D., Tyagarajan, S., Vachal, P. & Krska, S. W. The medicinal chemist's toolbox for late stage functionalization of drug-like molecules. *Chem. Soc. Rev.* **45**, 546–576 (2016).
7. Witt, K. A., Gillespie, T. J., Huber, J. D., Egleton, R. D. & Davis, T. P. Peptide drug modifications to enhance bioavailability and blood-brain barrier permeability. *Peptides* **22**, 2329–2343 (2001).
8. Räder, A. F. B. et al. Orally active peptides: is there a magic bullet? *Angew. Chem. Int. Ed.* **57**, 14414–14438 (2018).
9. Craik, D. J., Fairlie, D. P., Liras, S. & Price, D. The future of peptide-based drugs. *Chem. Biol. Drug Des.* **81**, 136–147 (2013).
10. Kimball, D. B., Herges, R. & Haley, M. M. Two unusual, competitive mechanisms for (2-ethynylphenyl)triazene cyclization: pseudo-coarctate versus pericyclic reactivity. *J. Am. Chem. Soc.* **124**, 1572–1573 (2002).
11. Young, B. S., Herges, R. & Haley, M. M. Doubly coarctate-stabilized carbenes: synthetic and computational studies. *J. Org. Chem.* **78**, 1977–1983 (2013).
12. McClintock, S. P., Forster, N., Herges, R. & Haley, M. M. Synthesis of α-ketoester- and α-hydroxyester-substituted isoindazoles via the thermodynamic coarctate cyclization of ester-terminated azo-ene-yne systems. *J. Org. Chem.* **74**, 6631–6636 (2009).
13. Herges, R. Coarctate and pseudocoarctate reactions: stereochemical rules. *J. Org. Chem.* **80**, 11869–11876 (2015).
14. Bucher, G., Heitmann, G. & Herges, R. Thermochemistry and photochemistry of spiroketals derived from indan-2-one: stepwise processes versus coarctate fragments. *Beilstein J. Org. Chem.* **9**, 1668–1676 (2013).
15. Kimball, D. B., Weakley, T. J. R. & Haley, M. M. Cyclization of 1-(2-Alkynylphenyl)-3,3-dialkyltriazenes: a convenient, high-yield synthesis of substituted cinnolines and isoindazoles. *J. Org. Chem.* **67**, 6395–6405 (2002).
16. Qiu, S., Gao, X. & Zhu, S. Dirhodium (ii)-catalysed cycloisomerization of azaenyne: rapid assembly of centrally and axially chiral isoindazole frameworks. *Chem. Sci.* **12**, 13730–13736 (2021).
17. Vitaku, E., Smith, D. T. & Njardarson, J. T. Analysis of the structural diversity, substitution patterns, and frequency of nitrogen heterocycles among U.S. FDA approved pharmaceuticals. *J. Med. Chem.* **57**, 10257–10274 (2014).
18. Jampilek, J. Heterocycles in medicinal chemistry. *Molecules* **24**, 3839 (2019).
19. Heravi, M. M. & Zadsirjan, V. Prescribed drugs containing nitrogen heterocycles: an overview. *RSC Adv.* **10**, 44247–44311 (2020).
20. Kerru, N., Gummidi, L., Maddila, S., Gangu, K. K. & Jonnalagadda, S. B. A review on recent advances in nitrogen-containing molecules and their biological applications. *Molecules* **25**, 1909 (2020).
21. Shirtcliff, L. D. et al. Biscyclization reactions in butadiyne- and ethyne-linked triazenes and diazenes: concerted versus stepwise coarctate cyclizations. *J. Am. Chem. Soc.* **128**, 9711–9721 (2006).
22. McClintock, S. P., Zakharov, L. N., Herges, R. & Haley, M. M. Coarctate versus pericyclic reactivity in naphthalene-fused

azo–ene–ynes: synthesis of benzocinnolines and benzoisoindazoles. *Chem. Eur. J.* **17**, 6798–6806 (2011).
23. Roughley, S. D. & Jordan, A. M. The medicinal chemist's toolbox: an analysis of reactions used in the pursuit of drug candidates. *J. Med. Chem.* **54**, 3451–3479 (2011).
24. Cramer, J., Sager, C. P. & Ernst, B. Hydroxyl groups in synthetic and natural-product-derived therapeutics: a perspective on a common functional group. *J. Med. Chem.* **62**, 8915–8930 (2019).
25. Zayed, M. E. M., El-Shishtawy, R. M., Elroby, S. A., Al-Footy, K. O. & Al-amshany, Z. M. Experimental and theoretical study of donor-π-acceptor compounds based on malononitrile. *Chem. Cent. J.* **12**, 26 (2018).
26. Grimm, J. B. et al. A general method to optimize and functionalize red-shifted rhodamine dyes. *Nat. Methods* **17**, 815–821 (2020).
27. Liu, H., Jiang, G., Ke, G., Ren, T. & Yuan, L. Organic fluorophores with large stokes shift for bioimaging and biosensing. *ChemPhotoChem* **8**, e202300277 (2024).
28. Zhou, L. et al. Rational development of near-infrared fluorophores with large stokes shifts, bright one-photon, and two-photon emissions for bioimaging and biosensing applications. *Chem. Eur. J.* **23**, 8736–8740 (2017).
29. Gao, Z., Hao, Y., Zheng, M. & Chen, Y. A fluorescent dye with large Stokes shift and high stability: synthesis and application to live cell imaging. *RSC Adv.* **7**, 7604–7609 (2017).
30. Pan, X., Zhao, Y. Q., Hu, F. Y., Chi, C. F. & Wang, B. Anticancer activity of a hexapeptide from skate (Raja porosa) cartilage protein hydrolysate in HeLa cells. *Mar. Drugs* **14**, 153 (2016).
31. Tougou, K., Nakamura, A., Watanabe, S., Okuyama, Y. & Morino, A. Paraoxonase has a major role in the hydrolysis of prulifloxacin (NM441), a prodrug of a new antibacterial agent. *Drug. Metab. Dispos.* **26**, 355–359 (1998).
32. Knadler, M. P., Lobo, E., Chappell, J. & Bergstrom, R. Duloxetine. *Clin. Pharmacokinet.* **50**, 281–294 (2011).
33. Vong, K., Yamamoto, T., Chang, T.-C. & Tanaka, K. Bioorthogonal release of anticancer drugs via gold-triggered 2-alkynylbenzamide cyclization. *Chem. Sci.* **11**, 10928–10933 (2020).
34. Marble, D. A. & Bosso, J. A. Norfloxacin: a quinoline antibiotic. *Drug Intell. Clin. Pharm.* **20**, 261–266 (1986).
35. Hingorani, D. V. et al. Monomethyl auristatin antibody and peptide drug conjugates for trimodal cancer chemo-radio-immunotherapy. *Nat. Commun.* **13**, 3869 (2022).
36. Dal Corso, A. et al. Advanced pyrrolidine-carbamate self-immolative spacer with tertiary amine handle induces superfast cyclative drug release. *ChemMedChem* **17**, e202200279 (2022).
37. Liu, C., Lv, J., Luo, S. & Cheng, J. P. $Sc(OTf)_3$-catalyzed transfer diazenylation of 1,3-dicarbonyls with triazenes via N–N Bond. *Org. Lett.* **16**, 5458–5461 (2014).
38. Li, F., Jiang, T., Li, Q. & Ling, X. Camptothecin (CPT) and its derivatives are known to target topoisomerase I (Top1) as their mechanism of action: did we miss something in CPT analogue molecular targets for treating human disease such as cancer? *Am. J. Cancer Res.* **7**, 2350–2394 (2017).
39. Weinstain, R., Slanina, T., Kand, D. & Klán, P. Visible-to-NIR-light activated release: from small molecules to nanomaterials. *Chem. Rev.* **120**, 13135–13272 (2020).
40. Kessler, M., Glatthar, R., Giese, B. & Bochet, C. G. Sequentially photocleavable protecting groups in solid-phase synthesis. *Org. Lett.* **5**, 1179–1181 (2003).
41. Wang, Y. et al. Peptide–drug conjugates as effective prodrug strategies for targeted delivery. *Adv. Drug Deliv. Rev.* **110**, 112–126 (2017).
42. Cao, Y., Luo, C., Yang, P., Li, P. & Wu, C. Indazole scaffold: a generalist for marketed and clinical drugs. *Med. Chem. Res.* **30**, 501–518 (2021).

Acknowledgements

This research was supported by NIH (grant No. 1R01HG012941-01) and NSF (Grant No. CHE-2406996 to M.R.). Monika Raj, Ph.D. was supported by a Research Scholar Grant, RSG-22-025-01-CDP, from the American Cancer Society.

Author contributions

S.S., Z.E.P., P.C., and M.R. designed the project. S.S. and Z.E.P. carried out small molecules scope, amino acids scope, fluorophore scope, linear peptide isoindazole scope, and optimized N-N bond cleavage. S.S. synthesized fluorescent peptides for cellular imaging, performed dual-tagging of peptides, and utilization of protective group for secondary amine. Z.E.P. discovered the photo-cleavage properties of the 2-amine-isoindazole, synthesized isoindazole drug conjugates, and performed chemoselectivity and 2-amine-isoindazole stability studies. J.M.T. performed all flow cytometry and cellular imaging studies. All authors wrote the manuscript. S.S. and Z.E.P. contributed equally. M.R. acquired funding and supervised the project.

Competing interests

The authors declare no competing interests.

Additional information

Supplementary information The online version contains supplementary material available at https://doi.org/10.1038/s41467-025-59057-x.

Correspondence and requests for materials should be addressed to Monika Raj.

Peer review information *Nature Communications* thanks Gonçalo Bernardes, who co-reviewed with Julie Becher, and the other, anonymous, reviewer(s) for their contribution to the peer review of this work. A peer review file is available.

Reprints and permissions information is available at http://www.nature.com/reprints

Publisher's note Springer Nature remains neutral with regard to jurisdictional claims in published maps and institutional affiliations.

Open Access This article is licensed under a Creative Commons Attribution-NonCommercial-NoDerivatives 4.0 International License, which permits any non-commercial use, sharing, distribution and reproduction in any medium or format, as long as you give appropriate credit to the original author(s) and the source, provide a link to the Creative Commons licence, and indicate if you modified the licensed material. You do not have permission under this licence to share adapted material derived from this article or parts of it. The images or other third party material in this article are included in the article's Creative Commons licence, unless indicated otherwise in a credit line to the material. If material is not included in the article's Creative Commons licence and your intended use is not permitted by statutory regulation or exceeds the permitted use, you will need to obtain permission directly from the copyright holder. To view a copy of this licence, visit http://creativecommons.org/licenses/by-nc-nd/4.0/.

© The Author(s) 2025